12-2023

Effects of the Build Orientation and Support Patterns on the Geometric Accuracy in Printing Parts With Overhang Structure: An Experimental Study

Bala Murali Krishna Mohan
The University of Texas Rio Grande Valley

EFFECTS OF THE BUILD ORIENTATION AND SUPPORT PATTERNS ON THE GEOMETRIC ACCURACY IN PRINTING PARTS WITH OVERHANG STRUCTURE: AN EXPERIMENTAL STUDY

A Thesis

by

BALA MURALI KRISHNA MOHAN

Submitted in Partial Fulfillment of the

Requirements for the Degree of

MASTER OF SCIENCE

Major Subject: Engineering Management

The University of Texas Rio Grande Valley

December 2023

EFFECTS OF THE BUILD ORIENTATION AND SUPPORT PATTERNS ON THE GEOMETRIC ACCURACY IN PRINTING PARTS WITH OVERHANG STRUCTURE: AN EXPERIMENTAL STUDY

A Thesis
by
BALA MURALI KRISHNA MOHAN

COMMITTEE MEMBERS

Dr. Yangyang Long
Chair of the Committee

Dr. Zhaohui Geng
Co-chair of the Committee

Dr. Jianzhi Li
Committee Member

Dr. Farid Ahmed
Committee Member

December 2023

ABSTRACT

Mohan, Bala Murali Krishna Build Orientation for Additive Manufactured Parts with Overhang Structures: An Experimental Study. Master of Science in Engineering Management (MSE), December 2023, 40 pp., 10 tables, 28 figures, 19 references, titles.

Additive manufacturing is becoming increasingly popular in industries such as manufacturing due to its ability to use raw materials more efficiently and require less machining than traditional methods(Calignano et al., 2017). However, constructing overhanging structures in additive manufacturing can be challenging, potentially affecting the overall geometric quality of the printed components. The objective of this study was to identify the most effective printing orientation for overhanging designs in Fused Deposition Modeling (FDM) using two different support structures. To achieve this, the researchers used a laser scanner to collect point cloud data and conducted a comparative study to determine the optimal orientation for the overhanging structures. The analysis revealed that the 45-degree overhang structure with grid support produced a good print result compared to other build orientations. Additionally, a comparison of FDM printed parts and L-PBF printed parts showed some similar noticeable defects.

DEDICATION

I dedicate this thesis to my outstanding professors, Dr. Zhaohui Geng, Dr. Yangyang Long, Dr. Jianzhi Li, and Dr. Farid Ahmed. Whose profound mentoring and advice have been the foundation of my academic development. I also owe a debt of gratitude to all my family members and friends, whose unflinching support, motivation, and confidence in my abilities have sustained me throughout this journey.

ACKNOWLEDGMENTS

I am deeply thankful to Dr. Zhaohui Geng for their unwavering support, guidance, and invaluable insights throughout the entire research process. His expertise and dedication have played a pivotal role in shaping the direction of this thesis.

I extend my appreciation to the members of my academic committee, Dr. Yangyang Long, Dr. Jianzhi Li, and Dr. Farid Ahmed for their thoughtful feedback and constructive criticism. Their expertise has greatly enriched the quality of this work.

I sincerely appreciate Oscar Martinez, Hernan Aparicio, Jorge Barron, and Jorge Mellado sharing the details of the L-PBF prints used in this study. The availability of these materials was instrumental in conducting thorough analyses and gaining valuable insights.

My sincere gratitude also goes to the National Institute of Standards and Technology under Grant No.70NANB21H038 and Greater Brownsville Incentive Cooperation, which supports our Future SQC projects.

With heartfelt gratitude,

Bala Murali Krishna Mohan

TABLE OF CONTENTS

Page

LIST OF TABLES

Page

LIST OF FIGURES

Page

CHAPTER I

INTRODUCTION

Additive manufacturing has gained significant popularity, and Fused Deposition Modeling (FDM) has become increasingly prevalent across various industries. It may be because of the flexibility of the manufacturing process and the ease of making the prototypes for the studies (Bourell et al., 2017). Printing complex designs has been easy using some parameters, like support structure and changing build orientation, but it also has some downsides. Sometimes, removing support structures may lead to poor surface quality. Getting accurate printed parts is challenging sometimes to achieve good print. Controlling the parameters can help achieve that, which is flexible due to the slicing software. Several studies have been done, and prints have been tested to control the parameters. Printing parameters change according to design and the complexity of the printing (Khan et al., 2021). Two kinds of accuracy inspections are performed on the printed portions of the 3D models: touch and non-contact techniques. Scanners are a quick and effective way to check the quality of completed printed parts (Almira et al., 2021.). There are different types of scanning metrology techniques available on the market. Laser scanners are one of the types that collect millions of reference points of surface data in real time. Point cloud data has the potential to be employed for a wide range of measures, which the utilization of specialized software can facilitate. The acquisition of point cloud data is essential to evaluating the precision of the manufactured components. Furthermore, point cloud data can

be employed for reverse engineering or generating digital world data, as exemplified by Geng and Bidanda (2021), who have proposed a metrological toolset based on three-dimensional point cloud data.

Additive Manufacturing

Additive manufacturing (AM) has garnered significant attention as a popular manufacturing technology. This technique uses a layer-by-layer material deposition process to build components. Parts are fabricated using 3D model data, minimizing the requirement for costly tools or molds. This manufacturing process is well-suited for producing high-complexity components in low-volume quantities (Calignano et al., 2017).

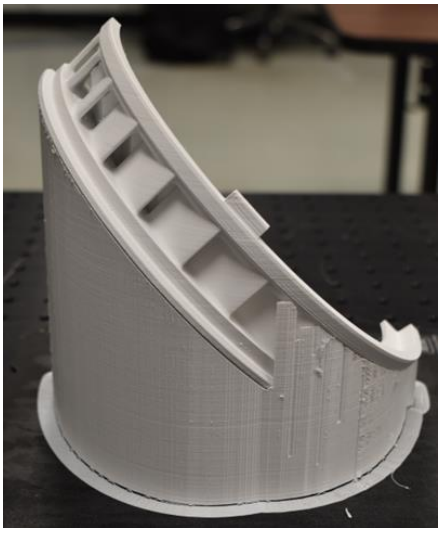

Figure 1: Additive print.

Various additive manufacturing processes are employed in the realm of manufacturing. The processes that fall under this category are vat photo-polymerization, sheet lamination, material extrusion, direct energy deposition, Laser-Powder Bed Fusion (L-PBF), and material jetting. The selection of materials for the additive manufacturing (AM) process depends on the specific technology employed. Polymers are often employed as a primary material for printing

due to their lightweight characteristics and ease of processing. Metals, either powder or wire, are frequently employed as materials in many applications. It must, however, be handled with extreme caution (Alfattni, 2022).

The AM process involves a step-by-step procedure from the CAD design to the final product. Firstly, the CAD design is converted into an STL file, which is then transformed into G-Code via slicer software. Next, machine setup takes place, which involves preparing the machine and inputting the G-Code. Once this is complete, the printing process commences, and post-processing of the printed part is the final step. The AM process has several advantages, including reduced lead time and suitability for producing complex components on demand. These benefits contribute to the reduction of storage requirements and material usage. Several drawbacks can be identified in the utilization of additive manufacturing techniques. Firstly, the surface finish quality achieved through these methods appears to be worse when compared to traditional manufacturing approaches.

Additionally, there are constraints on the limited selection of materials; the printing time required for additive manufacturing is typically more significant than that of conventional methods. Lastly, the initial setup expenses for equipment used in additive manufacturing are generally higher (Thomas, 2016). In this study, the fused deposition modeling process was used.

Fused Deposition Modeling (FDM)

FDM is an additive manufacturing technique that prints parts through a layer-by-layer deposition process. Molten polymer layer distribution was invented by Scott Crump in 1989 and is one of the more accessible techniques compared to other additive manufacturing techniques (Kuznetsov et al., 2018). There are a wide variety of materials available for FDM on the market. Some common materials are PLA, PETG, ABS, TPU, PC, ASA, and HIPS. The FDM printing

process is carried out in multiple phases, beginning with the design of STL files, 3D printers, G-code generation, and printing parameters, which are modified using slicing software for the different printing processes and materials. The nozzle is connected to the head of a 3D printer, and its temperature can be controlled via G-code or manually. The temperature may vary depending on the filament material, so it must be determined based on the material. The filament is connected to the nozzle using feeders.

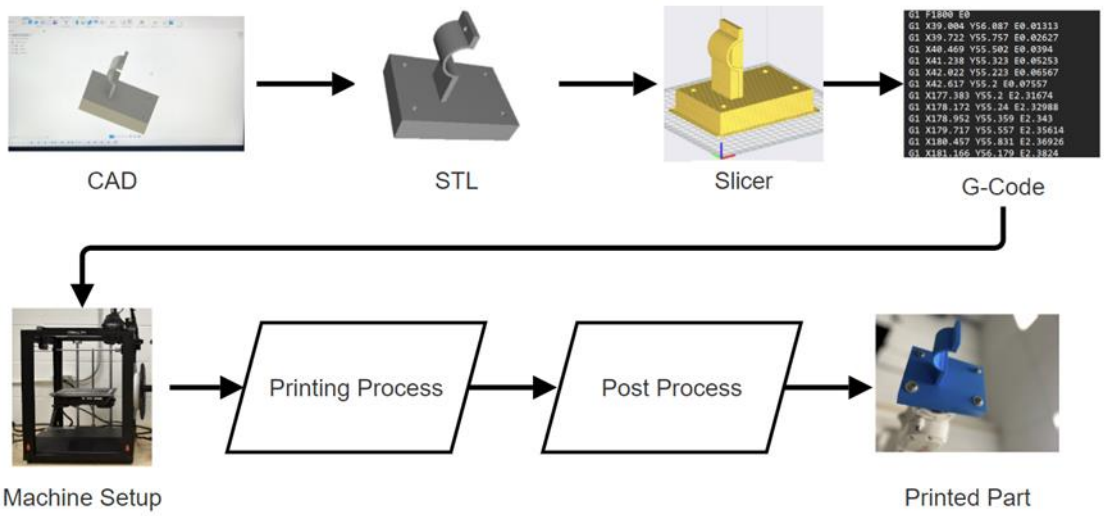

Figure 2: FDM process overview.

The filament will dissolve and pass through the nozzle due to the temperature and flow rate, and the feeder can control it. In order to print, the head moves in the XY plane, whereas the deposition base (bed) moves in the Z (vertical) orientation of the FDM schematic diagram (Harshitha & Rao, 2019). Various factors can affect the quality of prints, such as the thickness of layers, percentage of infill, and infill pattern. Additionally, the design of the component, specifically the presence of overhanging structures, can affect the outcome by resulting in poor geometry. Although support structures can assist overhanging structures, they may also result in a poor surface finish. This study utilized the FDM process to print the overhang with a support

structure on the base area. Different build orientations and different support patterns were used in the study. A laser scanner collected the printed parts' surface point cloud data. From the collected point cloud data, the deviation measurement of the printed part with the design model will be generated using the dedicated software. Then, those data will be analyzed using the statistical models.

Background investigation

The process parameters of additive printing significantly impact the geometry of the manufactured parts (Popescu et al., 2018). A study conducted by Dezaki et al. (2021) investigated the effects of infill pattern and infill density on the surface quality and mechanical properties of CAD-generated models and FDM-printed objects. The study found that CAD-generated models had slightly improved surface quality with circular and grid patterns. Maurya et al. (2022) compare the effects of differences in infill density and infill pattern on printing time and dimensional accuracy. The results show that 20% infill density and a hexagonal filler pattern are the most effective configurations while increasing infill density leads to printing delays. Buj-Corral et al. (2019) utilized a geometric model that computes the arithmetical mean height roughness parameter (Ra) for various print orientations between 5° and 85° using the mean value theorem for integrals. Results indicate that print orientation angles play a crucial role in surface roughness in the FDM-printed part (Jiang et al., 2018).

Fifty-seven papers on support optimization, which elaborated on the critical role of support structures in the additive manufacturing process, were examined in the review. It highlights the role of support structures in balancing the printing component and aiding in thermal dissipation. Di Angelo et al. (2020) proposed a method to find reliable build orientation for additive manufacturing applications, considering both surface quality and manufacturing cost

as factors. Additionally, the proposed method considers the effect of support structures on the additive manufacturing process. Nevertheless, the impact of the support method on the surface quality is not considered. In the study conducted by Delfs et al. (2016), simulation was employed to optimize the orientation of parts and other manufacturing parameters to enhance surface quality and minimize expenses associated with post-processing. Several variables considered for the simulation include layer thickness, build angle, and particle size. Matos et al. (2020) predict the optimal build orientation using an algorithm similar to that of electromagnetism, which Birbil and Fang created. The algorithm presented in this study aims to optimize multiple aspects that impact the quality of the manufactured product. These elements include volumetric error, support area, staircase effect, build time, surface roughness, and surface quality. Results indicate that the optimization of many objectives has negative consequences. The optimization of a single aim impacts the remaining objectives. According to Öteyaka et al. (2022), the infill pattern and infill ratio affect the strength of the printed part. This conclusion was reached by performing bending and hammer tests. Another study has shown that the build orientation, raster direction angle, and layer thickness significantly impact the accuracy of printed parts. The study used two types of PLA: one was white and heavy, while the other was lightweight and black (Hanon et al., 2021).

Research Goal

Based on the literature review, the research aims to explore whether keeping other parameters constant and only changing the build orientation and support patterns has a significant effect on overhanging additive prints. The research question of this study is presented as follows:

1. How the geometric accuracy of FDM printed parts with overhang structures be affected by building orientation and support patterns?
2. Can the knowledge extracted from FDM prints regarding geometric discrepancies or defects be transferred to other AM processes (L-PBF)?

CHAPTER II

METHODOLOGY

Fabrication of overhanging structures in the FDM Machine

Utilizing Creality Ender 5 S1 3D printers, the manufacturing of overhanging structures was accomplished. MakerBot Polylactic Acid (PLA) 1.75-mm-diameter filament was selected as the optimal material for achieving the desired outcomes. This filament is widely employed in FDM, making it one of the most popular materials for this application. Please refer to Table 1 to understand the filament's characteristics comprehensively. In this investigation, Creality Slicer 4.8.2 was utilized to manage printing parameters effectively. Only the printing orientation and support pattern were altered, while all other parameters remained unchanged. Figure 4 shows the overhanging design used for this study.

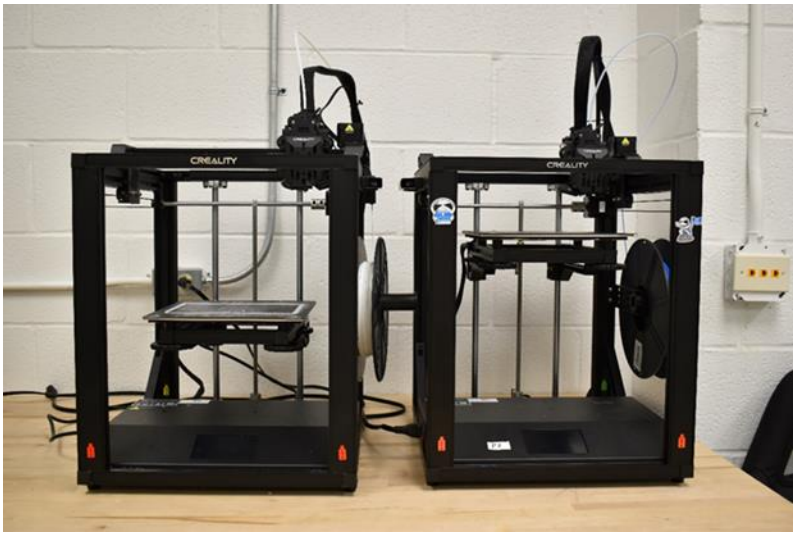

Figure 3: Creality Ender 5 S1 3D printers.

Table 1: PLA Properties

Properties	Value
Printing temperature	190–230°C
Printing speed	60–100 mm/s
Bed temperature	25–60°C

The parameters used were 40% infill, 0.1 profile, 0.1mm layer height, 1.2 wall thickness, cubic infill pattern, 200°C printing temperature, 75mm/s printing speed, and brim build plate adhesion. These parameters were carefully maintained throughout the process.

Figure 4: CAD Design.

Printing Strategy

In these studies, a factor screening process was employed to determine which factors were suitable for experimental printing. This process involved testing different build orientations, including 30, 40, 45, 50, and 60 degrees, as well as four distinct support patterns: grid, concentric, cross, and gyroid. The purpose of the screening was to eliminate any factors that would negatively impact printability.

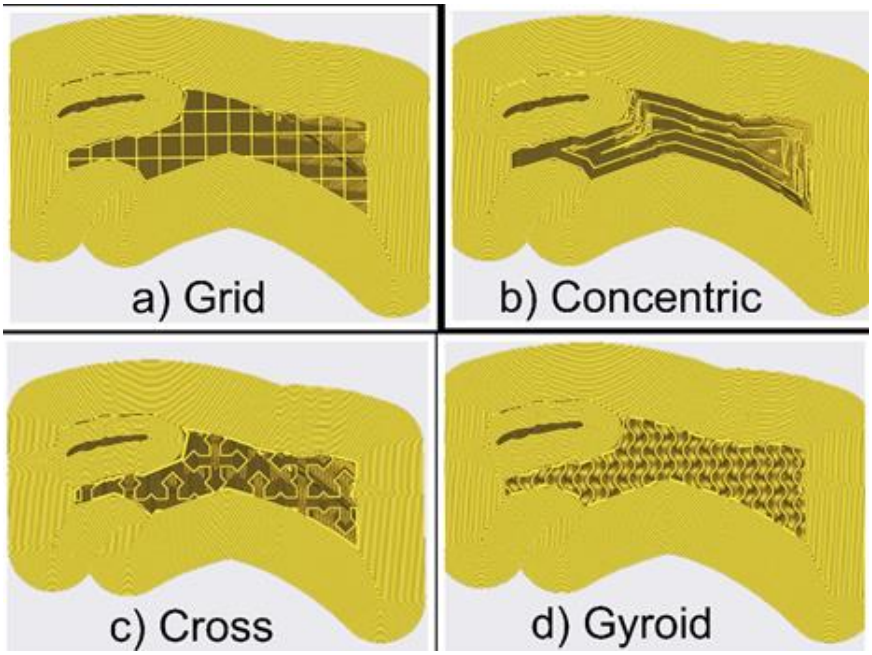

Figure 5: Types of support.

A total of 30 parts were printed, some with satisfactory results while others were suboptimal. Based on the outcome of the factors screening, grid, and cross-support patterns were selected for experimental printing. The results of the factor screening showed that the grid and cross-support patterns produced satisfactory prints in all build orientations compared to other support patterns.

Experimental printing

These experimental parts are printed randomly. The printing sequence is generated using the RAND() function in Excel. The same type of PLA was utilized for the pilot study and experimental parts. The following images illustrate various printed components characterized by diverse grid and cross-support patterns. Specifically, Figures 6 and 8 depict six parts of parts 1 and 2, respectively, featuring a grid support system. On the other hand, Figures 7 and 9 showcase six parts of part 1 and part 2 with cross support. Part 1 mentions that the first part is printed at that angle, and a support pattern follows for Part 2.

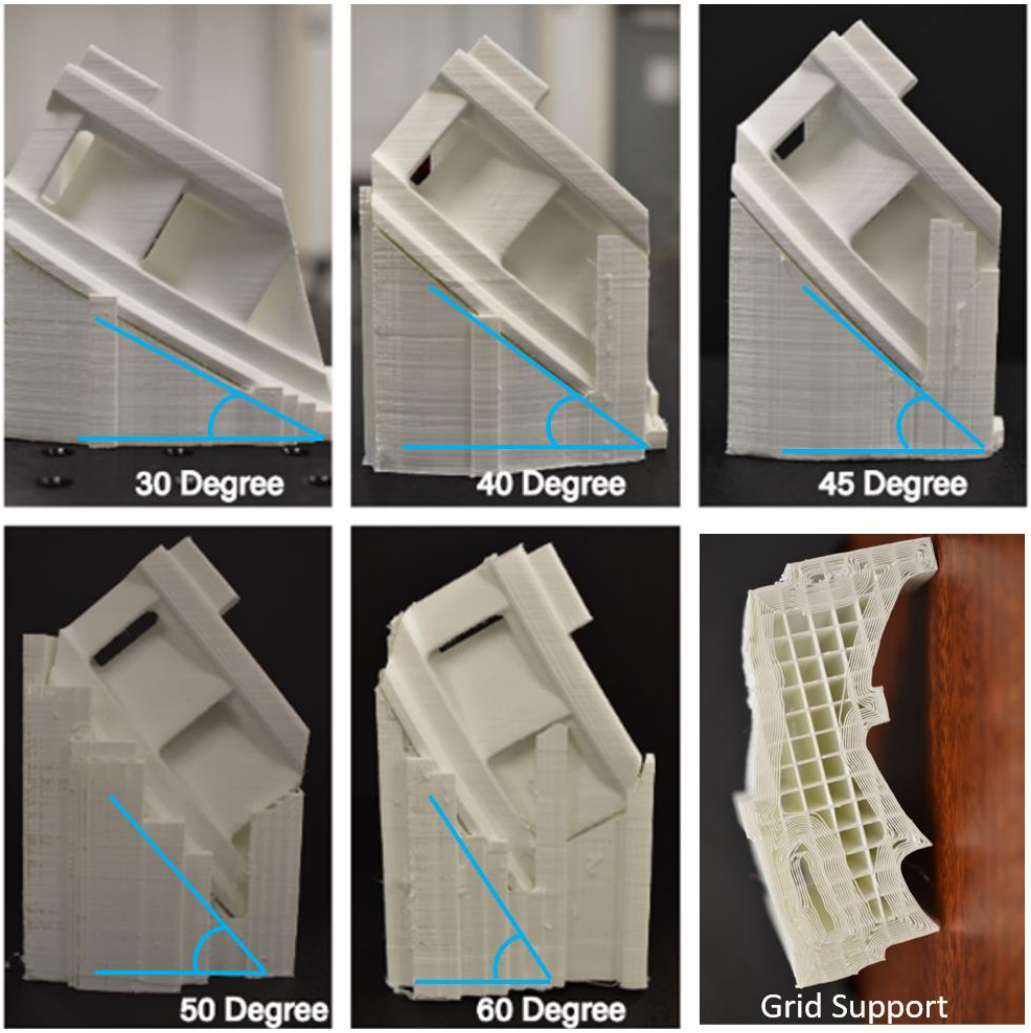

Figure 6: Part-1 Grid-support pattern.

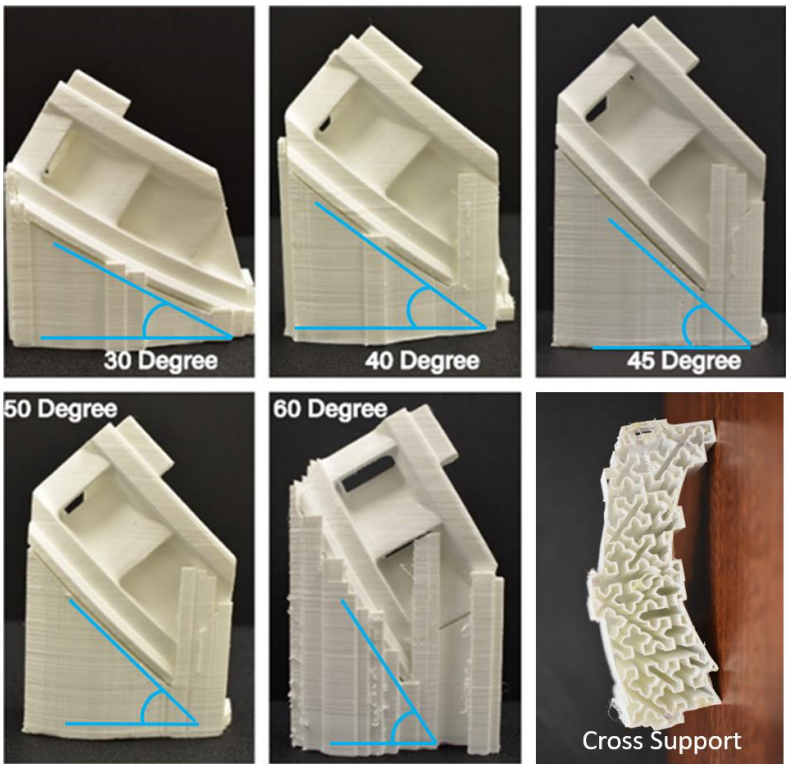

Figure 7: Part-1 Cross-support pattern.

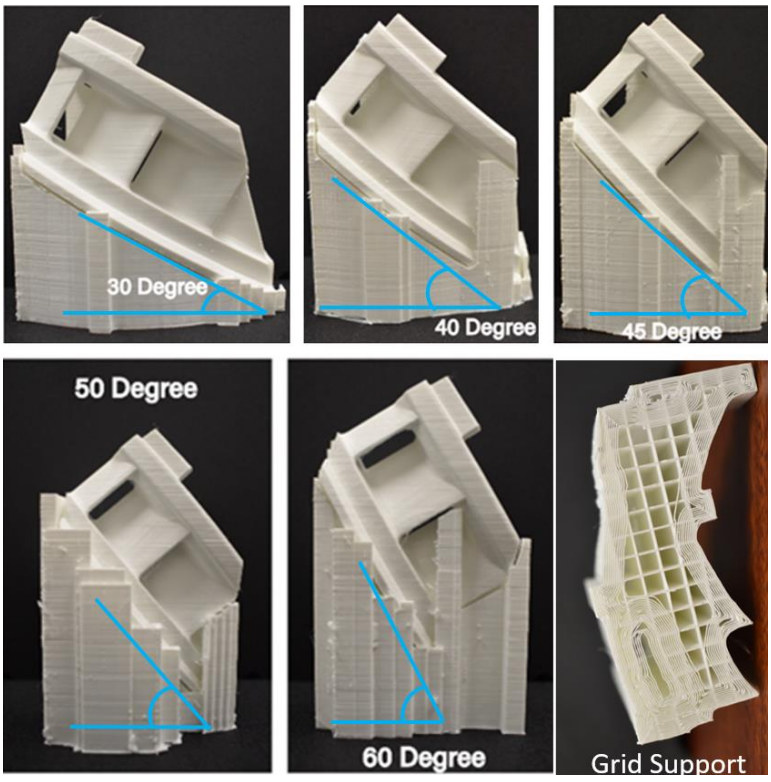

Figure 8: Part-2 Grid-support pattern.

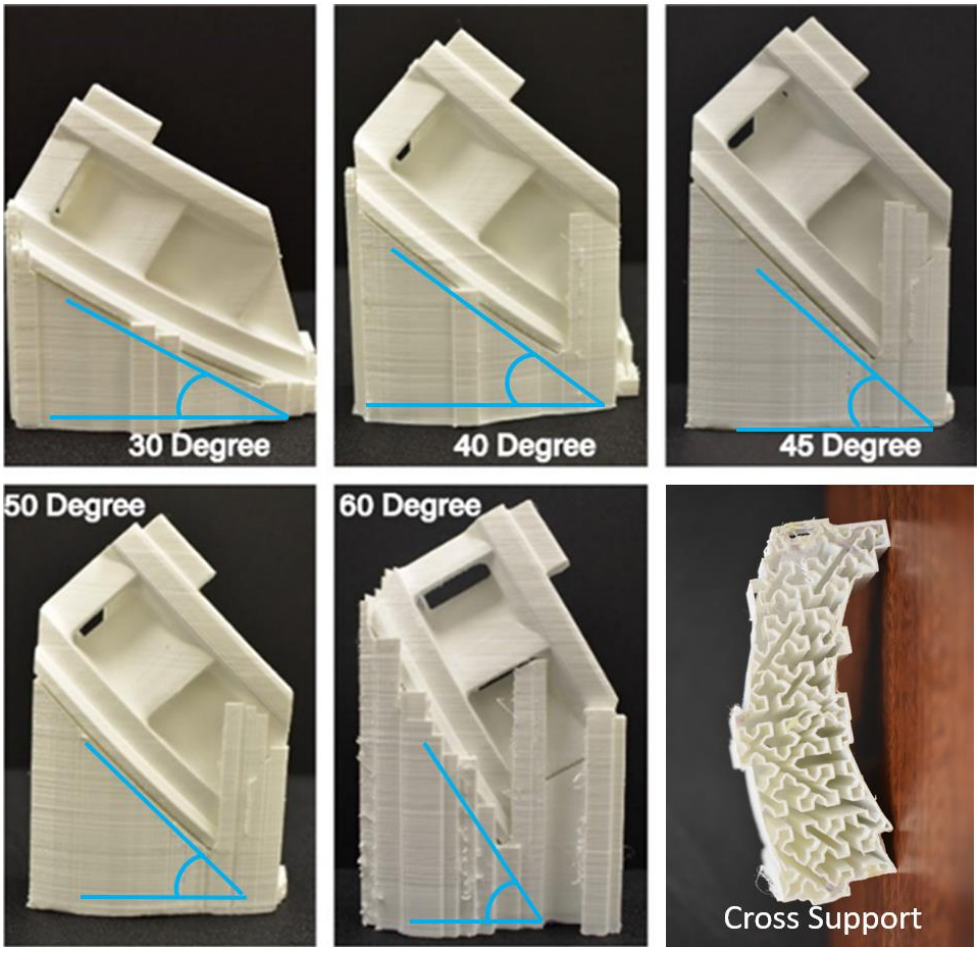

Figure 9: Part-2 Cross-support pattern.

Point Cloud Collection

In order to gather data, we utilized a Hexagon laser scanner to obtain point clouds of twenty printed components. The scanning procedure was done on each component, leading to the generation of a point cloud file utilizing the PC-DMIS 2023.2 software. The scanner arm has been securely positioned on the optical table, designed to minimize vibrations. The scanning component was positioned in the custom-printed section and firmly attached to the optical table using bolts. The scanner arm and laptop were connected according to the manual. Then, the

scanner arm was calibrated by following the procedure in the manual PC-DMIS for Arms 102 – Scanning v2023.1.


Figure 10: HEXAGON absolute arm.

Scanning Steps:

The scanning process involved, according to the guidelines outlined in the manual, ensuring the appropriate configuration: Active profile as Default, Exposure as Auto, and Pre-Defined Scanning Profile as COP - Standard Resolution.

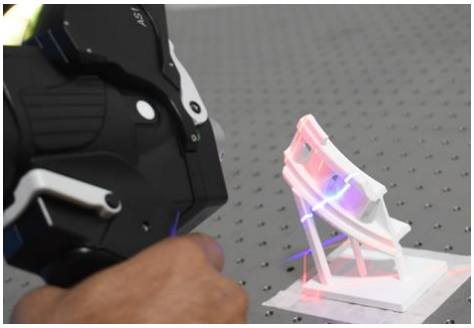
Figure 11: Process To Collect Point Clouds

In order to incorporate a random element into the scanning process, the RAND () function was employed. Following the completion of all required setups, the scanning process started with the following steps:

1. The measurement was set to millimeters, and the file was created with the name of the scan piece.
2. To generate an exclusion plane, begin by thoroughly scanning the custom-printed fixture. Upon activation of the exclusion plane, the point-cloud data situated below a designated plane offset will be automatically eliminated. The table or fixture is excluded from the scan file. The exclusion scanning offset setting was configured to be 20 millimeters.
3. The initiation and performance of the scanning process for the printed part were carried out with extreme caution. During the scanning process, we were able to inspect the scanning region visually by paying attention to the laptop display. Upon the completion of the scan, all regions of the printed part were thoroughly covered with points.
4. Approximately 5 million points were gathered, and all of the data was saved.

The same procedure was followed for all twenty printed parts. After collecting the point clouds for each printed part, the noise created in every file was meticulously cleaned using PCDMIS software.

Point Cloud Filter and Align

Once the scanning procedure was finished, each file was opened individually. All unwanted points were then selected and removed using the Point Cloud Filtering algorithm. Once the extraneous data was removed, further procedures were carried out to align the point cloud with the computer-aided design (CAD) model using the Iterative Closest Point algorithm (ICP) with a pre-set threshold.

1. The process of importing a CAD IGES file and subsequently selecting the CAD, followed by applying the surface vector option to fix the vectors, has significant importance. The presence of incorrect vectors can have a major effect on alignment; hence, rectifying them is the highest priority.
2. The Auto function was used to align the point cloud and CAD after the surface vector was fixed using the CAD alignment option.
3. Once the alignment process was concluded, the Point Cloud/CAD Alignment tool displayed the outcomes resulting from average deviation, maximum deviation, and standard deviation. These three steps were performed on all twenty components, and the results have been recorded for further investigation.

Surface Colormap

A surface colormap is used to compare the computer-aided design (CAD) model and the printed component by utilizing various colors. The various color visualizations show the areas of variation, displaying the highest and lowest levels of deviation alongside well-defined sections. Additionally, it offers a distribution curve and the corresponding distribution percentages for the given component. Colormaps were developed for each of the twenty components.

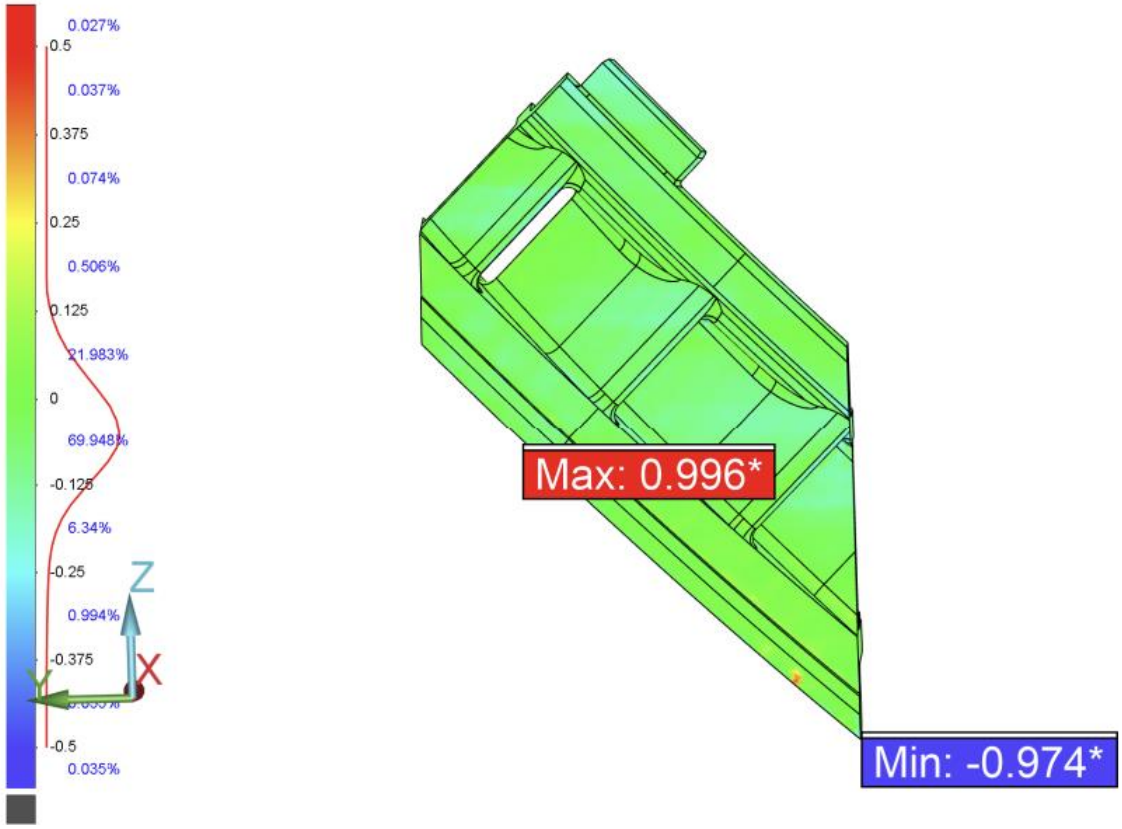

Figure 12: Colormap

CHAPTER III

RESULTS AND DISCUSSION

Below, the colormap's findings are examined. Twenty colormaps were subjected to detailed examination; the color green denotes a point close to the nominal design, whereas the color red represents a large positive deviation, and the color blue represents a large negative deviation, and a distribution curve is constructed to show the deviation distribution among all the points in the survey point cloud.

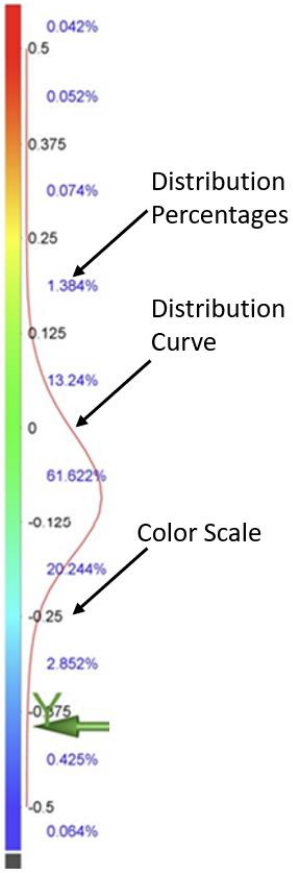

Figure 13: Distribution Curve

Surface Colormap

30-degree Build Orientation

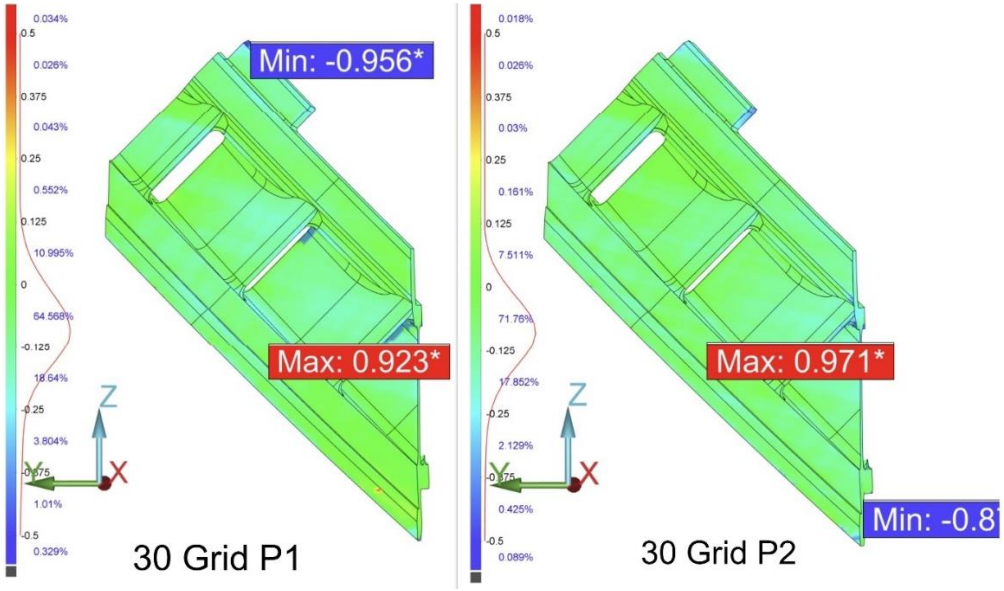

Figure 14: 30-degree grid-support pattern colormap

If we examine the outcomes of the 30-degree Grid P1 and the 30-degree Grid P2, In the interval scale of +0.5mm to +0.375mm, P1 has 0.026% compared to P2's 0.026% at the upper tail of the distribution curve, and with a deviation interval of -0.375mm to -0.5mm in the scale, P1 has 1.01% compared to P2's 0.425%. At the maximum deviation curve (0 to -0.125mm), P1 has an area of 64.568%, while P2 has an area of 71.76%. The percentage of P1 and P2 occurrences near zero is 79.271% and 75.563%, respectively, within the interval scale of +0.125mm to -0.125mm.

For 30-degree Cross P1 and the 30-degree Cross P2 in the interval scale of +0.5mm to +0.375mm, P1 has 0.11% compared to P2's 0.054% at the upper tail of the distribution curve, and in the interval scale of -0.375mm to -0.5mm, P1 has 0.757% compared to P2's 0.362%. At the maximum deviation curve (0 to -0.125mm), P1 has an area of 59.332%, while P2 has an area

of 66.616%. The percentage of P1 and P2 occurrences near zero is 79.776% and 75.563%, respectively, within the interval of +0.125mm to -0.125mm.

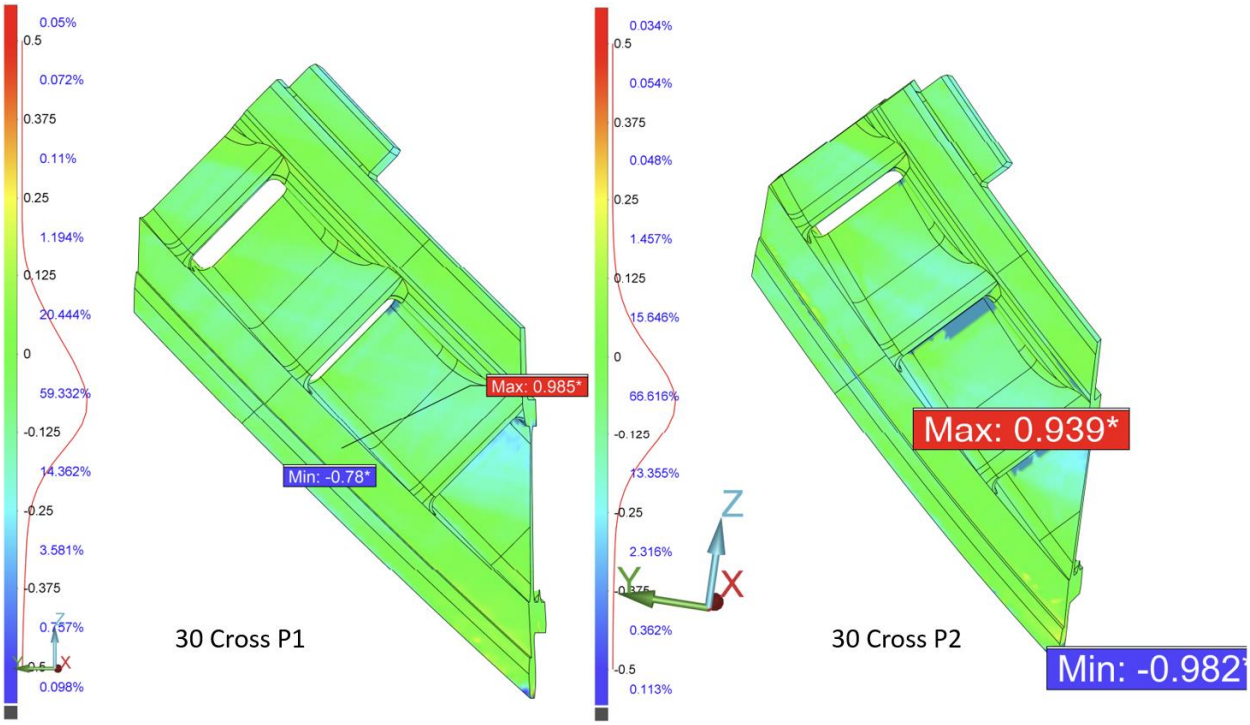

Figure 15: 30-degree cross-support pattern colormap.

40-degree Build Orientation

In the 40-degree grid support parts, 83.373% and 78.461% were printed in intervals of +0.125mm to -0.125mm for 40-degree P1 and 40-degree P2, respectively. In the interval of +0.5mm to +0.375mm, P1 has 0.058% compared to P2's 0.03% at the distribution curve upper tail, and in the interval of -0.375mm to -0.5mm on the scale, P1 has 0.33% compared to P2's 0.355%. At the maximum deviation area (0 to -0.125mm), P1 has an area of 67.987%, while P2 has an area of 65.483%.

For 40-degree Cross P1 and the 40-degree Cross P2 interval of +0.5mm to +0.375mm, P1 has 0.024% compared to P2's 0.052% at the distribution curve upper tail, and in the interval scale of -0.375mm to -0.5mm, P1 has 0.527% compared to P2's 0.362%. The percentage of P1 and P2

occurrences near zero is 73.73% and 74.862%, respectively, within the interval scale of +0.125mm to -0.125mm.

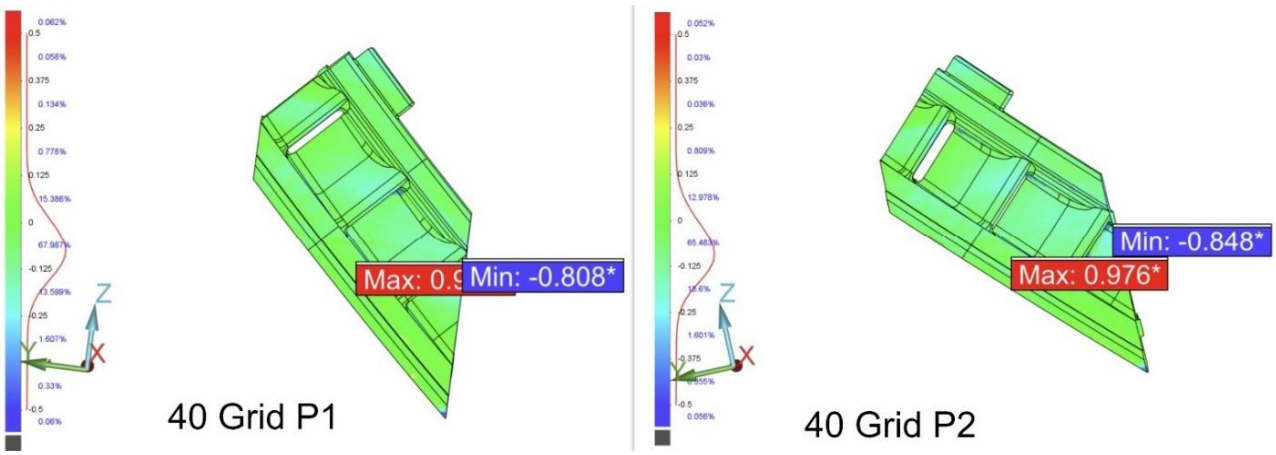

Figure 16: 40-degree grid-support pattern colormap.

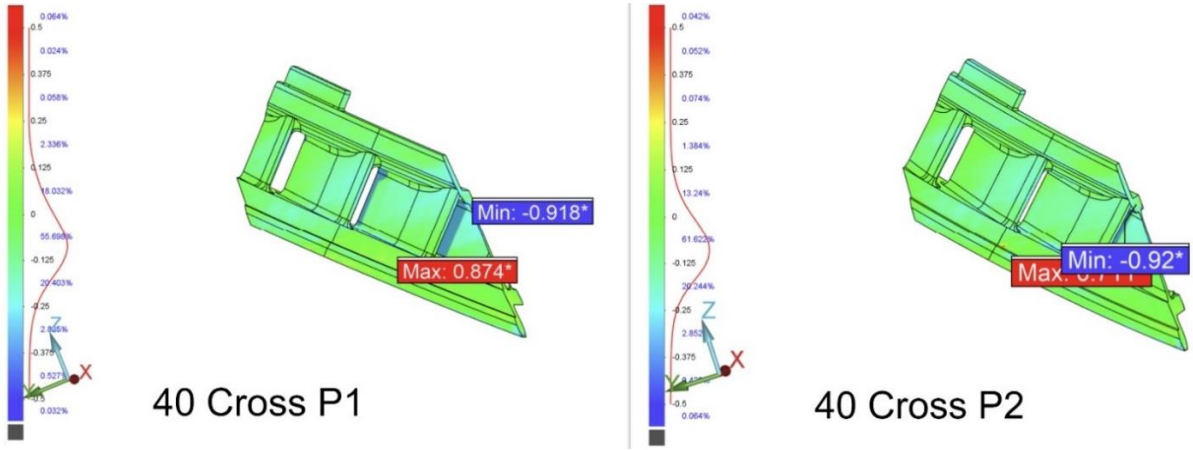

Figure 17: 40-degree cross-support pattern colormap.

45-degree Build Orientation

While 45-degree Grid P1 and 45-degree Grid P2 have an interval of +0.5mm to +0.375mm in scale, P1 has 0.037% compared to P2's 0.045% at the upper tail of the distribution curve, and in the interval of -0.375mm to -0.5mm, P1 has 0.375% compared to P2's 0.197%. The

percentage of P1 and P2 occurrences near zero is 91.931% and 93.122%, respectively, within the interval of +0.125mm to -0.125mm.

45-degree Cross P1 and 45-degree Cross P2 in the interval of +0.5mm to +0.375mm, P1 has 0.039% compared to P2's 0.346% at the upper tail, and in the interval of -0.375mm to -0.5 mm, P1 has 0.199% compared to P2's 2.169%. The percentage of P1 and P2 occurrences near zero is 84.002% and 66.924%, respectively, within the interval of +0.125mm to -0.125mm.

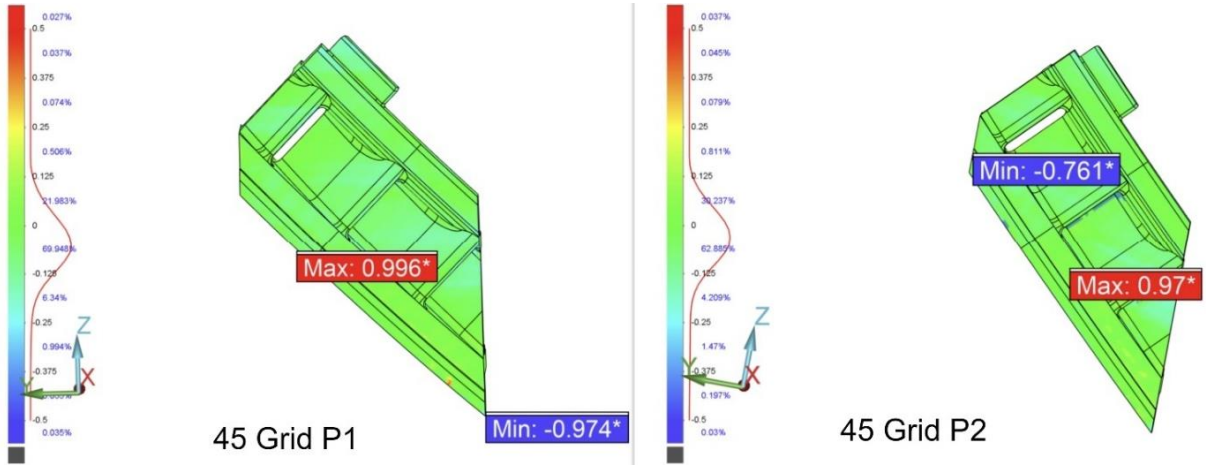

Figure 18: 45-degree grid support pattern colormap.

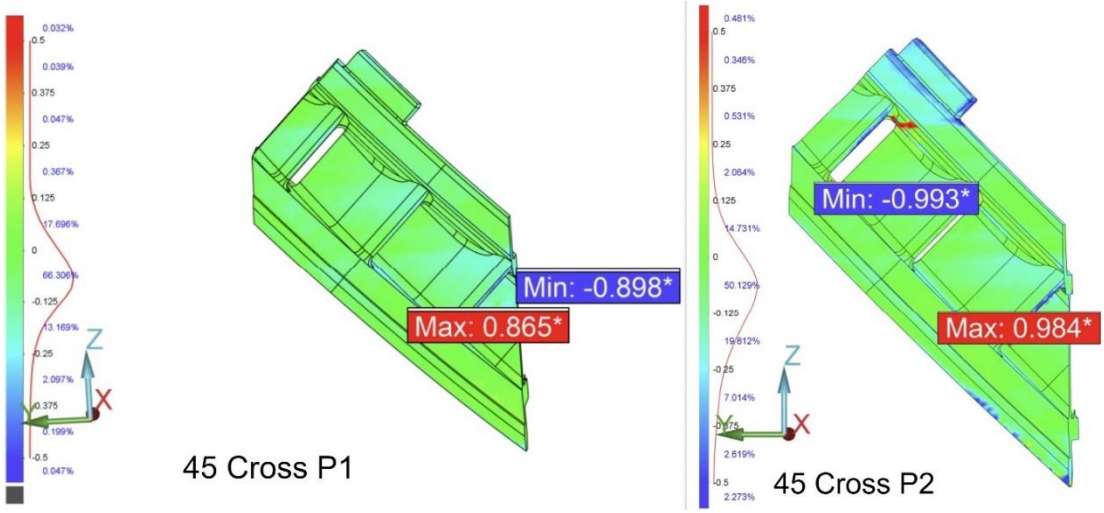

Figure 19: 45-degree cross-support pattern colormap.

50-degree Build Orientation

For the 50-degree Grid P1 and the 50-degree Grid P2, in the interval of +0.5mm to +0.375mm, P1 has 0.034% compared to P2's 0.03% at the upper tail, and in the interval of -0.375mm to -0.5mm, P1 was 0.427% compared to P2's 0.401%. The percentage of P1 and P2 occurrences near zero is 79.736% and 72.25%, respectively, within the interval of +0.125mm to -0.125mm.

50-degree Cross P1 and 50-degree Cross P2 in the interval of +0.5mm to +0.375mm, P1 has 0.026% compared to P2's 0.028% at the upper tail, and in the interval of -0.375mm to -0.5mm, P1 has 0.367% compared to P2's 0.188%. The percentage of P1 and P2 occurrences near zero is 79.793% and 75.463%, respectively, within the interval of +0.125mm to -0.125mm.

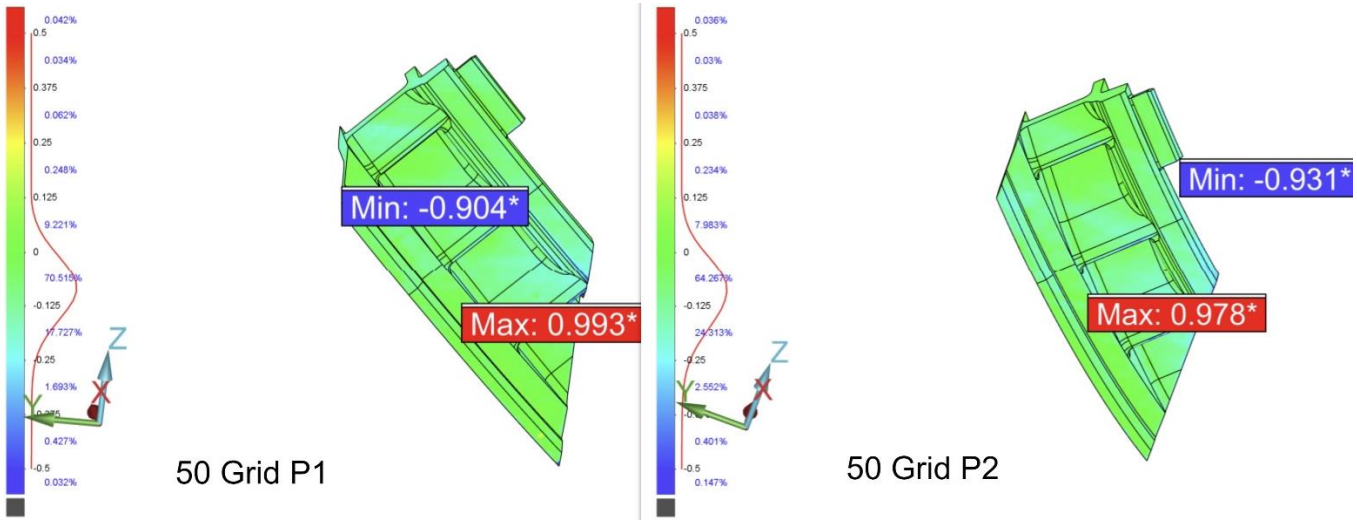

Figure 20: 50-degree grid support pattern colormap.

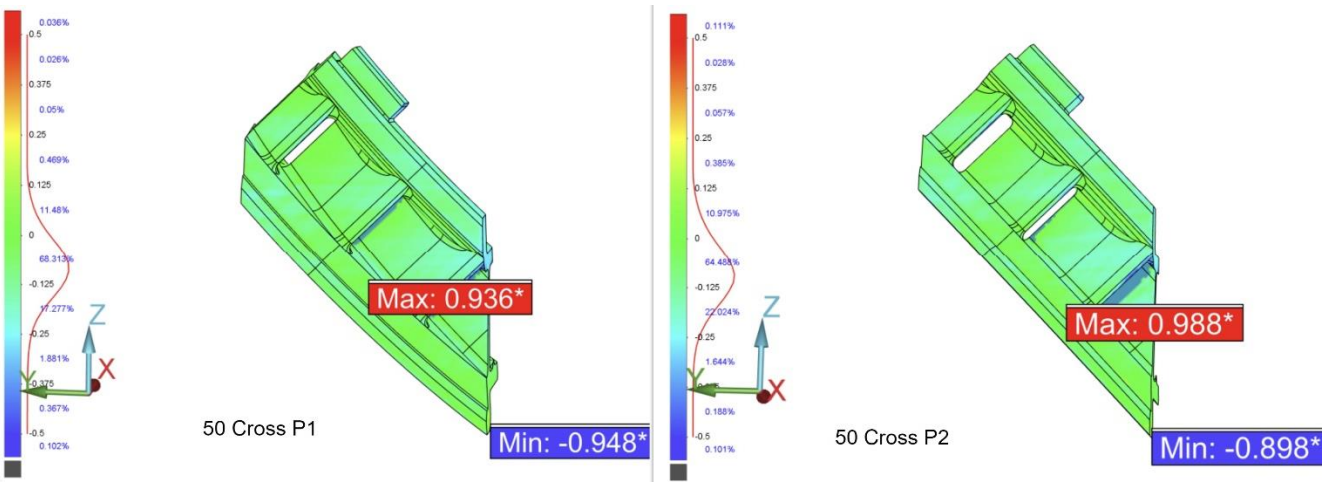

Figure 21: 50-degree cross-support pattern colormap.

60-degree Build Orientation

The final orientation of 60-degree grid support parts, 84.498% and 80.042%, was printed in the interval of +0.125mm to -0.125mm for 60-degree P1 and 60-degree P2. In the interval of +0.5mm to +0.375mm, P1 has 0.033% compared to P2's 0.026% at the upper tail, and in the interval of -0.375mm to -0.5mm, P1 has 0.21% compared to P2's 0.226%.

For 60-degree Cross P1 and the 60-degree Cross P2 in an interval of +0.5mm to +0.375mm, P1 has 0.093% compared to P2's 0.026% at the upper tail, and in the interval of -0.375mm to -0.5mm, P1 has 0.21% compared to P2's 0.345%. The percentage of P1 and P2 occurrences near zero is 73.498% and 85.297%, respectively, within the interval of +0.125mm to -0.125mm.

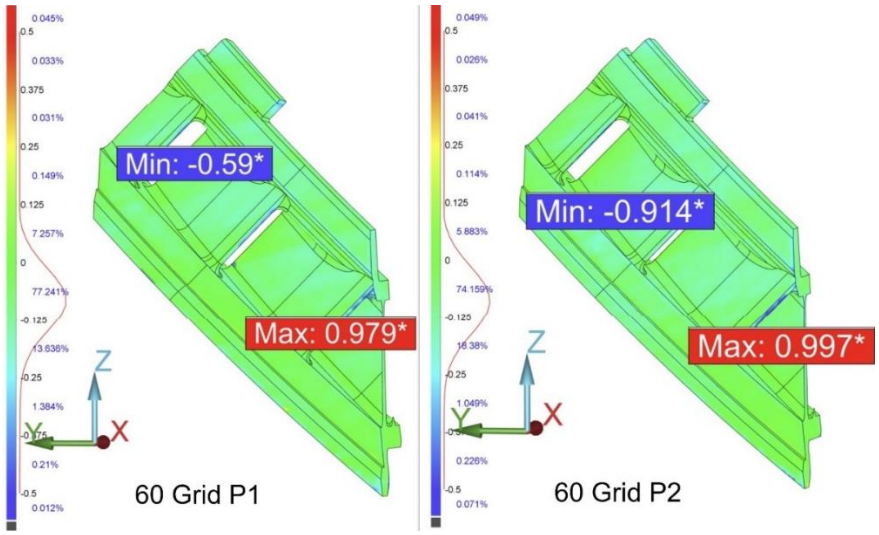

Figure 22: 60-degree grid support pattern colormap.

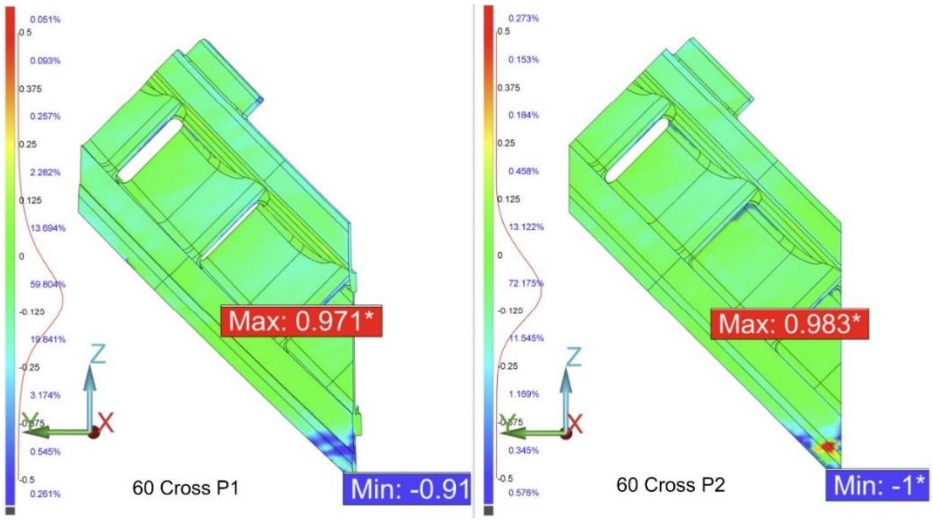

Figure 23: 60-degree cross-support pattern colormap.

The colormaps reveal the presence of common defects in the lower-end section of the part. The shape of the design in this section is curved and pointed, which is a result of the limited resolution available from FDM printing.

Robust Accuracy Metric

When it comes to evaluating printing accuracy, instead of assessing the overall performance of all the points, a reliable and effective approach is to use a predefined tolerance specification as a robust metric. This allows for a more precise and detailed comparison of the printing accuracy. From the colormap data, we determined the percentage of good printing area for each part. It falls between the areas of +0.125mm and -0.125mm. Using that data, when we perform the plot band graph, it will give a good result regarding orientation and support pattern. For performing this graph, the data was grouped into two sets of data: grid and cross-support.

Table 2: Values b/w +0.125mm to -0.125mm

Tolerance range +0.125mm to -0.125 mm					
Build Orientation (Degree)	30	40	45	50	60
Grid Part 1	79.271%	83.373%	91.931%	79.736%	84.498%
Grid Part 2	75.563%	78.461%	93.122%	72.25%	80.042%
Cross Part 1	79.776%	73.73%	84.002%	79.793%	73.498%
Cross Part 2	75.563%	74.862%	66.924%	75.463%	85.297%

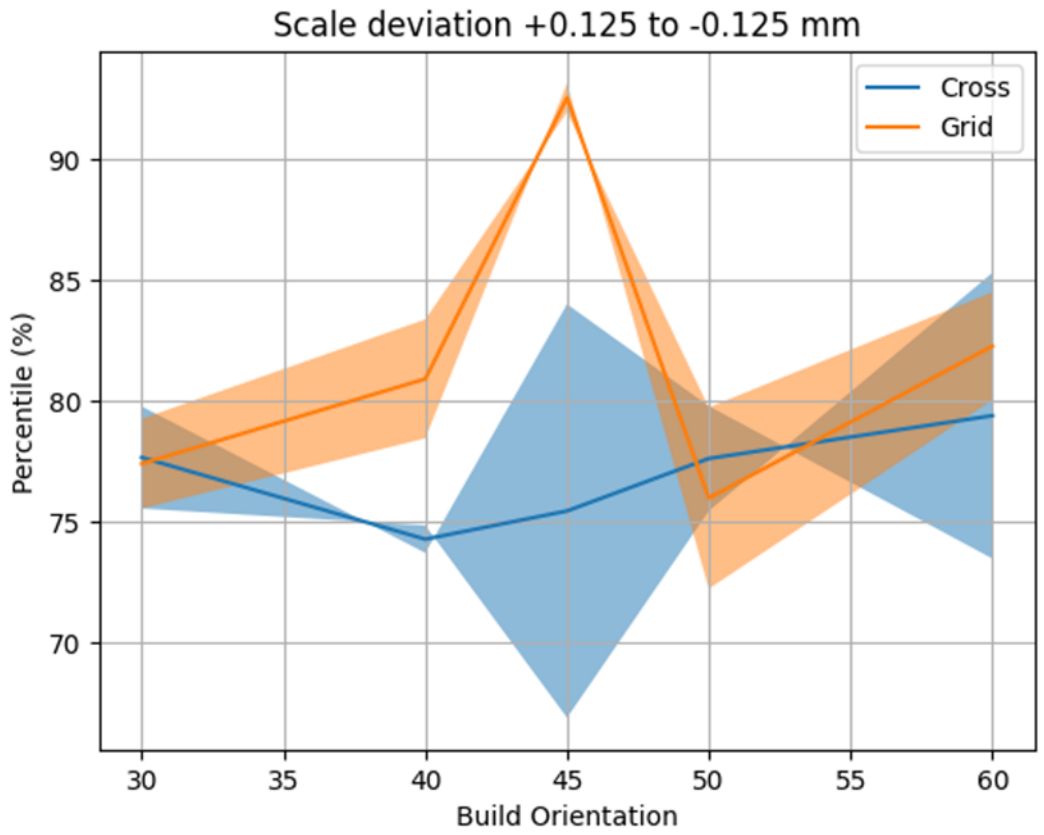

Figure 24: Tolerance Range Graph.

As for the grid support, the most accurate print seems to be around 45 degrees with low variability, which is a local optimal within the range from 30 to 60. Regarding cross support, the build orientation on the boundary seems to provide the most precise print, although it still has considerable variability. In build orientation of 60 degrees for grid and cross support, the graph shows an upward trend, but printing overhanging parts above 60 degrees becomes more difficult due to their overhanging structure.

ANOVA

A general two-way factorial ANOVA is used to evaluate the main and interaction effects of two independent variables in our study, namely build orientation and support pattern. These two factors have five and two levels, respectively. The ANOVA analysis is conducted using Minitab. The analysis is carried out using the following accuracy metrics:

1. Mean deviation
2. Standard deviation
3. Maximum deviation
4. Minimum deviation
5. Tolerance Range (Percentage value covers an interval of +0.125 to -0.125)

When computing the CAD design and point cloud, we obtain the accuracy metrics data: mean deviation, standard deviation, maximum deviation, and minimum deviation. The values are shown below:

Table 3: Accuracy Metrics Values

Mean			
Angle	Support	P1	P2
30	Grid	0.095	0.107
40	Grid	0.096	0.099
45	Grid	0.074	0.075
50	Grid	0.097	0.101
60	Grid	0.092	0.093

Mean			
Angle	Support	P1	P2
30	Cross	0.104	0.098
40	Cross	0.107	0.107
45	Cross	0.09	0.13
50	Cross	0.095	0.105
60	Cross	0.116	0.092

Std Dev			
Angle	Support	P1	P2
30	Grid	0.117	0.138
40	Grid	0.13	0.127
45	Grid	0.103	0.114
50	Grid	0.129	0.127
60	Grid	0.12	0.118

Std Dev			
Angle	Support	P1	P2
30	Cross	0.143	0.131
40	Cross	0.136	0.136
45	Cross	0.121	0.188
50	Cross	0.122	0.134
60	Cross	0.152	0.131

Maximum			
Angle	Support	P1	P2
30	Grid	0.971	0.923
40	Grid	0.945	0.976
45	Grid	0.996	0.97
50	Grid	0.993	0.978
60	Grid	0.979	0.997

Maximum			
Angle	Support	P1	P2
30	Cross	0.985	0.939
40	Cross	0.874	0.711
45	Cross	0.865	0.984
50	Cross	0.936	0.988
60	Cross	0.971	0.983

Minimum			
Angle	Support	P1	P2
30	Grid	-0.873	-0.956
40	Grid	-0.808	-0.848
45	Grid	-0.974	-0.761
50	Grid	-0.904	-0.931
60	Grid	-0.59	-0.914

Minimum			
Angle	Support	P1	P2
30	Cross	-0.78	-0.982
40	Cross	-0.918	-0.92
45	Cross	-0.898	-0.993
50	Cross	-0.948	-0.898
60	Cross	-0.916	-1

Once the values were obtained, the general factorial design was performed using this information to find the optimal build orientation. In the general factorial design, two factors were performed using Minitab® 21.4.2.

1. General Factorial Regression: Mean versus Build Orientation, Support Pattern.
2. General Factorial Regression: Standard deviation versus Build Orientation, Support Pattern.
3. General Factorial Regression: Maximum deviation versus Build Orientation, Support Pattern.
4. General Factorial Regression: Minimum deviation versus Build Orientation, Support Pattern.
5. General Factorial Regression: Tolerance range versus Build Orientation, Support Pattern. The results are shown below.

Statistical Analysis

General Factorial Regression: Mean versus Build Orientation, Support Pattern

Table 4: Accuracy Metric Mean

Source	DF	Adj SS	Adj MS	F-Value	P-Value
Model	9	0.001725	0.000192	1.54	0.254
Linear	5	0.000903	0.000181	1.45	0.287
Build Orientation	4	0.000241	0.00006	0.49	0.746
Support Pattern	1	0.000661	0.000661	5.33	0.044
2-Way Interactions	4	0.000823	0.000206	1.66	0.236
Build Orientation*Support Pattern	4	0.000823	0.000206	1.66	0.236
Error	10	0.001241	0.000124		
Total	19	0.002967			

The influence of Build Orientation, Support Pattern, and their interaction on the mean has revealed that the build orientation does not have a significant effect on the mean, whereas the support pattern has a statistically significant effect at the 0.05 level of significance.

General Factorial Regression: Standard Deviation versus Build Orientation, Support Pattern

Table 5: Accuracy Metric Standard Deviation

Source	DF	Adj SS	Adj MS	F-Value	P-Value
Model	9	0.00282	0.000313	1.08	0.449
Linear	5	0.001513	0.000303	1.04	0.444
Build Orientation	4	0.000051	0.000013	0.04	0.996
Support Pattern	1	0.001462	0.001462	5.04	0.049
2-Way Interactions	4	0.001307	0.000327	1.13	0.397
Build Orientation*Support Pattern	4	0.001307	0.000327	1.13	0.397
Error	10	0.002899	0.00029		
Total	19	0.005719			

Based on the analysis of Build Orientation, Support Pattern, and their interaction, it has been found that the standard deviation is not affected significantly by the build orientation.

However, the support pattern has been observed to have a statistically significant effect with a P-value of 0.049 at the 0.05 level of significance.

General Factorial Regression: Maximum Deviation versus Build Orientation, Support Pattern

Table 6: Accuracy Metric Maximum Deviation

Source	DF	Adj SS	Adj MS	F-Value	P-Value
Model	9	0.06071	0.006745	2.69	0.07
Linear	5	0.04027	0.008053	3.21	0.055
Build Orientation	4	0.02816	0.007041	2.81	0.085
Support Pattern	1	0.0121	0.012103	4.82	0.053
2-Way Interactions	4	0.02044	0.00511	2.04	0.165
Build Orientation*Support Pattern	4	0.02044	0.00511	2.04	0.165
Error	10	0.02509	0.002509		
Total	19	0.0858			

The influence of the build orientation and support pattern on maximum deviation was analyzed, revealing P values of 0.085 and 0.053 at the 0.05 level of significance.

General Factorial Regression: Minimum versus Build Orientation, Support Pattern

Table 7: Accuracy Metric Minimum Deviation

Source	DF	Adj SS	Adj MS	F-Value	P-Value
Model	9	0.06892	0.007658	0.7	0.699
Linear	5	0.03505	0.007011	0.64	0.675
Build Orientation	4	0.01097	0.002743	0.25	0.903
Support Pattern	1	0.02408	0.024082	2.2	0.169
2-Way Interactions	4	0.03387	0.008468	0.77	0.567
Build Orientation*Support Pattern	4	0.03387	0.008468	0.77	0.567
Error	10	0.10948	0.010948		
Total	19	0.1784			

Analyzing the build orientation and support pattern interaction on minimum deviation, we obtained P values of 0.903 and 0.169 at the 0.05 level of significance.

Tolerance range Versus Build Orientation, Support Pattern

Table 8: Accuracy Metric Tolerance Range

Source	DF	Adj SS	Adj MS	F-Value	P-Value
Model	9	492.1	54.68	1.87	0.171
Linear	5	267.8	53.57	1.83	0.194
Build Orientation	4	146.1	36.53	1.25	0.351
Support Structure	1	121.7	121.72	4.17	0.068
2-Way Interactions	4	224.3	56.07	1.92	0.184
Build Orientation*Support Structure	4	224.3	56.07	1.92	0.184
Error	10	291.9	29.19		
Total	19	784			

The influence of build orientation, support pattern, and their interaction on the tolerance range has revealed that the build orientation and support pattern have a P value of 0.351 and 0.068 at the 0.05 level of significance, respectively.

More investigation is needed, so a one-way ANOVA was performed separately for the tolerance range of the grid, and cross-supports using Minitab were used to evaluate statistically significant variations in the average values of support patterns across different levels of the build orientation.

One-way ANOVA for Grid support

Table 9: One-way ANOVA for Grid Support

Source	DF	Adj SS	Adj MS	F-Value	P-Value
Build Orientation	4	337.97	84.49	7.34	0.025
Error	5	57.6	11.52		
Total	9	395.57			

One-way ANOVA for Grid support tolerance value as a response and the P-value 0.025 shows that the build orientation is statistically significant at a significant level 0.05. Fisher pairwise shows that the impact of the 45-degree build orientation is statistically different from other build orientations.

One-way ANOVA for cross-support

Table 10: One-way ANOVA for Cross Support

Source	DF	Adj SS	Adj MS	F-Value	P-Value
Build Orientation	4	157.6	39.4	1.81	0.265
Error	5	109.1	21.83		
Total	9	266.7			

At a significant level of 0.05, the build orientation P value for the cross-support tolerance range is 0.265 based on one-way ANOVA. Comparing the results of a one-way ANOVA for Grid-support and cross-support. Grid support gives a significant result compared to cross-support. 45-degree build orientation gives a good print with a grid support P value of 0.025.

A paired T-test was performed to check whether grid and cross-support structures have statistically significant different impacts on the percentile value. T-value of 1.96 suggests some difference between groups.

Comparison of FDM-printed parts and Laser Powder Bed Fusion (L-PBF) prints.

The primary objective of this comparative analysis is to compare two different additive manufacturing techniques, Fused Deposition Modeling (FDM) printing, and Laser Powder Bed Fusion (L-PBF) printing, regarding their ability to produce identical designs. The objective of the

comparison is to evaluate the building orientation of the prints without considering the materials used. The study aims to identify any similar defects in the printed parts.

When comparing L-PBF parts and FDM parts, some defects in the parts are similar, and the vernier caliper was used to measure the defects. Below, the defects of different build orientations of FDM and L-PBF were examined.

30-degree FDM part vs. L-PBF part

The defect in the upper region of the 30-degree FDM P1 is similar to that observed in the upper region of the 30-degree L-PBF P1. The defect measured from the measuring origin for the FDM part is 16.5mm, while the defect measured from the measuring origin for the L-PBF is 17.2mm, as measured with a vernier caliper.

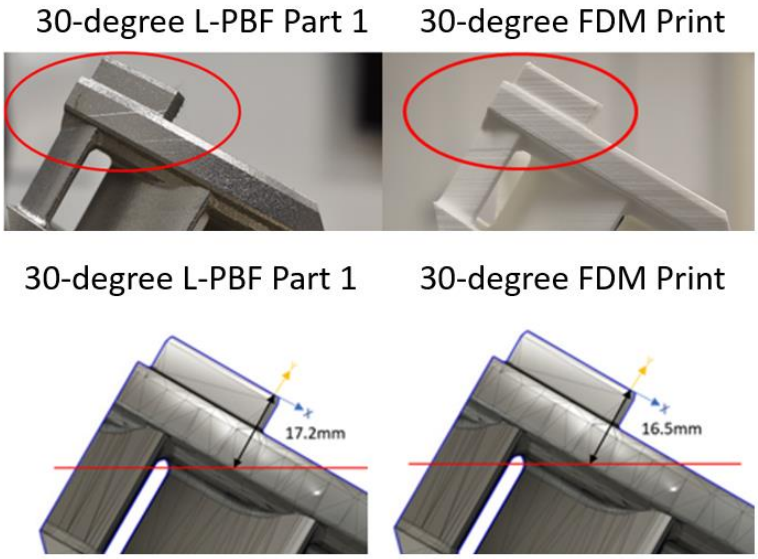

Figure 25: 30-degree L-PBF part 1 vs FDM Part.

During the comparison, an additional 30-degree parts were produced using L-PBF and FDM. Defects were observed in L-PBF Part 2 and the FDM print, occurring from the measurement origin at distances of 21.4 mm and 18.2 mm, respectively.

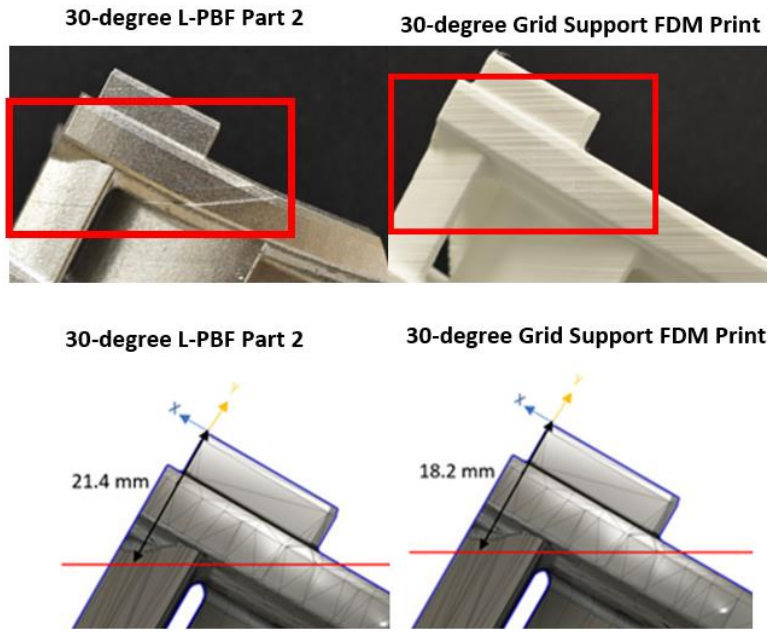

Figure 26: 30-degree FDM part vs. L-PBF part (2).

40-degree FDM part vs L-PBF part

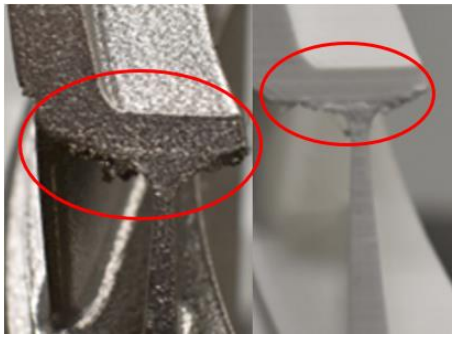
Figure 27: 40-degree L-PBF vs FDM

Compared to the L-PBF and FDM components, the bridge section at 40-degrees displays some drooping. This occurrence occurs due to the overhanging structure and significantly influences the quality of the printed components' surfaces.

50-degree FDM part vs. L-PBF part

A mid-section crack has been noticed in the 50-degree L-PBF parts. Similarly, the FDM part also has a defect in the mid-section. On measuring, it was found that the L-PBF defects occur from the measurement origin, 45.04mm; in the FDM, it is 44.2 mm.

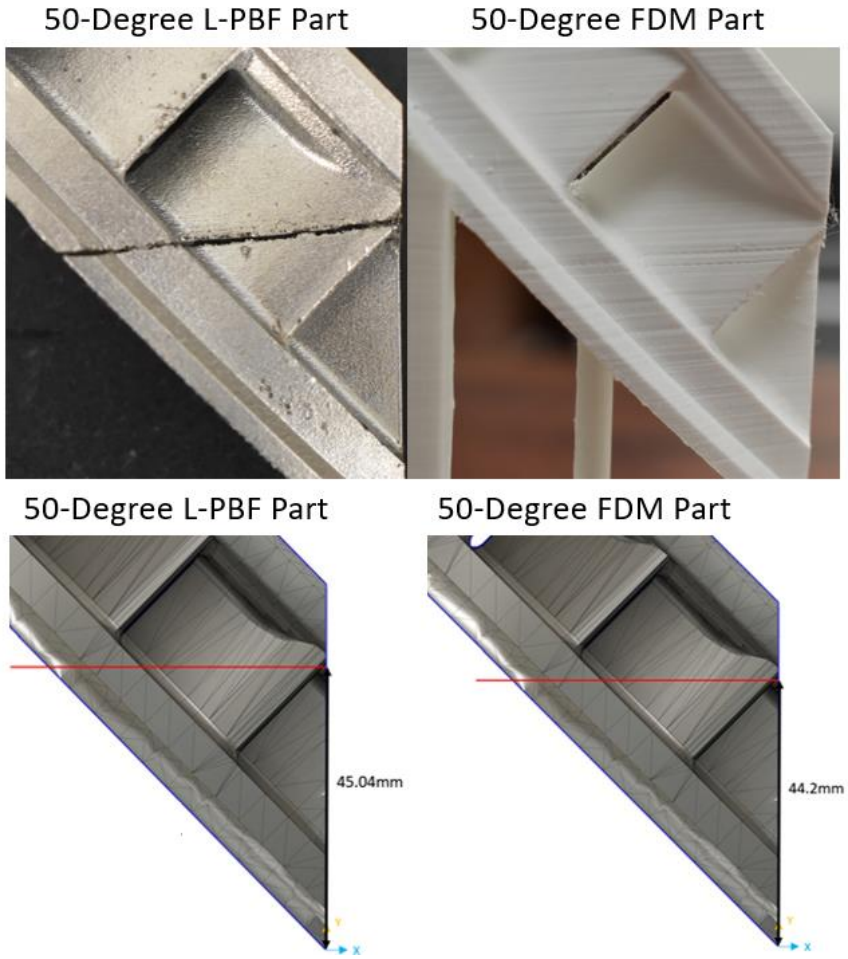

Figure 28: 50-degree FDM part vs. L-PBF part

CHAPTER IV

CONCLUSION AND FUTURE WORK

The results for design printed in the FDM process in this study show that in the robust accuracy metric, 45-degree with grid support gives a significant result. The ANOVA results show that at the statistical significance level of 0.05, support patterns have a significant impact on the accuracy metrics of mean and standard deviation, with P-values of 0.044 and 0.049. One-way ANOVA for grid support revealed a significant P value of 0.025 for build orientation. Furthermore, a paired T-test with a T-value of 1.69 indicates that there is a difference between grid and cross-support systems. From this result, the 45-degree build orientation and grid support pattern show good print results, which was aligned with the expert result who printed the full part. The comparison between L-PBF and FDM prints has revealed that the defect patterns in both techniques are comparable.

The ANOVA analysis has shown that in some of the accuracy metrics, the build orientation is not statistically significant at the statistical significance level of 0.05. Although visual inspections have identified some defects in the FDM, they are not reflected in the colormap deviation results that follow global geometric metrics. Therefore, to gain even more detailed information about the parts in future work, it is important to develop local geometric metrics that can identify local deviation patterns. Furthermore, a local registration algorithm must be implemented to detect these patterns effectively.

REFERENCES

Alfattni, R. (2022). Comprehensive Study on Materials used in Different Types of Additive Manufacturing and their Applications. *International Journal of Mathematical, Engineering and Management Sciences*, *7*(1), 92–114. https://doi.org/10.33889/IJMEMS.2022.7.1.007

Almira, S., Bašić, H., Softić, A., & Baljić, K. (n.d.). *A COMPARISON OF THE CMM AND MEASURING SCANNER FOR PRINTING PRODUCTS GEOMETRY MEASUREMENT*. https://www.researchgate.net/publication/355702358

Bourell, D., Kruth, J. P., Leu, M., Levy, G., Rosen, D., Beese, A. M., & Clare, A. (2017). Materials for additive manufacturing. *CIRP Annals - Manufacturing Technology*, *66*(2), 659–681. https://doi.org/10.1016/j.cirp.2017.05.009

Buj-Corral, I., Domínguez-Fernández, A., & Durán-Llucià, R. (2019). Influence of Print Orientation on Surface Roughness in Fused Deposition Modeling (FDM) Processes. *Materials*, *12*(23), 3834. https://doi.org/10.3390/ma12233834

Calignano, F., Manfredi, D., Ambrosio, E. P., Biamino, S., Lombardi, M., Atzeni, E., Salmi, A., Minetola, P., Iuliano, L., & Fino, P. (2017). Overview on additive manufacturing technologies. *Proceedings of the IEEE*, *105*(4), 593–612. https://doi.org/10.1109/JPROC.2016.2625098

Delfs, P., T̈ows, M., & Schmid, H. J. (2016). Optimized build orientation of additive manufactured parts for improved surface quality and build time. *Additive Manufacturing*, *12*, 314–320. https://doi.org/10.1016/j.addma.2016.06.003

Dezaki, M. L., Ariffin, M. K. A. M., Serjouei, A., Zolfagharian, A., Hatami, S., & Bodaghi, M. (2021). Influence of infill patterns generated by cad and fdm 3d printer on surface roughness and tensile strength properties. *Applied Sciences (Switzerland)*, *11*(16). https://doi.org/10.3390/app11167272

Di Angelo, L., Di Stefano, P., Dolatnezhadsomarin, A., Guardiani, E., & Khorram, E. (2020). A reliable build orientation optimization method in additive manufacturing: the application to FDM technology. *International Journal of Advanced Manufacturing Technology*, *108*(1–2), 263–276. https://doi.org/10.1007/S00170-020-05359-X/TABLES/7

Geng, Z., & Bidanda, B. (2021). Geometric precision analysis for Additive Manufacturing processes: A comparative study. *Precision Engineering*, *69*, 68–76. https://doi.org/10.1016/j.precisioneng.2020.12.022

Hanon, M. M., Zsidai, L., & Ma, Q. (2021). Accuracy investigation of 3D printed PLA with various process parameters and different colors. *Materials Today: Proceedings*, *42*, 489–3096. https://doi.org/10.1016/j.matpr.2020.12.1246

Harshitha, V., & Rao, S. S. (2019). Design and analysis of ISO standard bolt and nut in FDM 3D printer using PLA and ABS materials. *Materials Today: Proceedings*, *19*, 583–588. https://doi.org/10.1016/j.matpr.2019.07.737

Jiang, J., Xu, X., & Stringer, J. (2018). Support structures for additive manufacturing: A review. In *Journal of Manufacturing and Materials Processing* (Vol. 2, Issue 4). MDPI. https://doi.org/10.3390/jmmp2040064

Khan, S., Joshi, K., & Deshmukh, S. (2021). A comprehensive review on effect of printing parameters on mechanical properties of FDM printed parts. *Materials Today: Proceedings*, *50*, 2119–2127. https://doi.org/10.1016/j.matpr.2021.09.433

Kuznetsov, V. E., Solonin, A. N., Urzhumtsev, O. D., Schilling, R., & Tavitov, A. G. (2018). Strength of PLA components fabricated with fused deposition technology using a desktop 3D printer as a function of geometrical parameters of the process. *Polymers*, *10*(3). https://doi.org/10.3390/polym10030313

Matos, M. A., Rocha, A. M. A. C., & Pereira, A. I. (2020). Improving additive manufacturing performance by build orientation optimization. *International Journal of Advanced Manufacturing Technology*, *107*(5–6), 1993–2005. https://doi.org/10.1007/s00170-020-04942-6

Maurya, S., Malik, B., Sharma, P., Singh, A., & Chalisgaonkar, R. (2022). Investigation of different parameters of cube printed using PLA by FDM 3D printer. *Materials Today: Proceedings*, *64*, 1217–1222. https://doi.org/10.1016/j.matpr.2022.03.700

Öteyaka, M. Ö., Çakir, F. H., & Sofuoğlu, M. A. (2022). Effect of infill pattern and ratio on the flexural and vibration damping characteristics of FDM printed PLA specimens. *Materials Today Communications*, *33*. https://doi.org/10.1016/j.mtcomm.2022.104912

Popescu, D., Zapciu, A., Amza, C., Baciu, F., & Marinescu, R. (2018). FDM process parameters influence over the mechanical properties of polymer specimens: A review. *Polymer Testing*, *69*, 157–166. https://doi.org/10.1016/j.polymertesting.2018.05.020

Thomas, D. (2016). Costs, benefits, and adoption of additive manufacturing: a supply chain perspective. *International Journal of Advanced Manufacturing Technology*, *85*(5–8), 1857–1876. https://doi.org/10.1007/s00170-015-7973-6

BIOGRAPHICAL SKETCH

Bala Murali Krishna Mohan was born in Chennai, India on August 8, 1995. He grew up in Tamil Nadu (India), where he developed a passion for Manufacturing Engineering.

Bala Murali Krishna Mohan pursued his diploma studies in mechanical engineering at NPR Polytechnic College, graduating with a diploma in 2015. Then, he continued his academic journey and earned his undergraduate studies in mechanical engineering at NPR College of Engineering and Technology, graduating with a bachelor's degree in 2018. He then continued his academic journey and earned his master's degree in engineering management from the University of Texas Rio Grande Valley in 2023.

Bala Murali Krishna Mohan has a keen interest in additive manufacturing. He has extensively researched build orientation for additive manufactured parts with overhang structures—an experimental study during his academic career.

With a strong educational background, extensive research experience, and a passion for additive manufacturing, Bala Murali Krishna Mohan is dedicated to advancing knowledge in additive manufacturing. His commitment to academic excellence and innovative thinking make him a valuable contributor to the field.